Oxalate Decarboxylase and Oxalate Oxidase Activities Can Be Interchanged with a Specificity Switch of up to 282 000 by Mutating an Active Site Lid[†,‡]

Matthew R. Burrell, Victoria J. Just, Laura Bowater, Shirley A. Fairhurst, Laura Requena, David M. Lawson, and Stephen Bornemann*

Department of Biological Chemistry, John Innes Centre, Norwich Research Park, Norwich NR4 7UH, United Kingdom

Received May 17, 2007; Revised Manuscript Received August 6, 2007

ABSTRACT: Oxalate decarboxylases and oxalate oxidases are members of the cupin superfamily of proteins that have many common features: a manganese ion with a common ligand set, the substrate oxalate, and dioxygen (as either a unique cofactor or a substrate). We have hypothesized that these enzymes share common catalytic steps that diverge when a carboxylate radical intermediate becomes protonated. The *Bacillus subtilis* decarboxylase has two manganese binding sites, and we proposed that Glu162 on a flexible lid is the site 1 general acid. We now demonstrate that a decarboxylase can be converted into an oxidase by mutating amino acids of the lid that include Glu162 with specificity switches of 282 000 (SEN161-3DAS), 275 000 (SENS161-4DSSN), and 225 000 (SENS161-4DASN). The structure of the SENS161-4DSSN mutant showed that site 2 was not affected. The requirement for substitutions other than of Glu162 was, at least in part, due to the need to decrease the K_m for dioxygen for the oxidase reaction. Reversion of decarboxylase activity could be achieved by reintroducing Glu162 to the SENS161-4DASN mutant to give a relative specificity switch of 25 600. This provides compelling evidence for the crucial role of Glu162 in the decarboxylase reaction consistent with it being the general acid, for the role of the lid in controlling the K_m for dioxygen, and for site 1 being the sole catalytically active site. We also report the trapping of carboxylate radicals produced during turnover of the mutant with the highest oxidase activity. Such radicals were also observed with the wild-type decarboxylase.

The functionally diverse cupin superfamily of proteins is defined by a β-barrel fold together with a characteristic protein sequence motif (*1*−*3*). Oxalate decarboxylases and oxalate oxidases are members of this superfamily, and they share many common features, an involvement in stress responses (*1*, *4*), mononuclear manganese ions (*5*, *6*) coordinated by one Glu and three His residues (*7*−*10*), oxalate as a substrate, and dioxygen as either a unique cofactor (*6*, *11*) or a substrate, together with potential commercial applications (*1*, *2*). We proposed a divergent catalytic mechanism to account for the different outcomes to catalysis with these two similar enzymes (*6*). A number of studies have provided experimental and theoretical evidence (*10*, *12*−*16*) for some of the catalytic steps currently thought to be involved (Figure 1). We have hypothesized that the decisive step that directs catalysis toward decarboxylation would be the protonation of an enzyme-bound carboxylate (formyl) radical species (*6*) and that the general-acid catalyst would be Glu162 in the *Bacillus subtilis* OxdC decarboxylase (*9*). We have shown that the proton originally comes from solvent and that the Glu162 residue forms part of a flexible lid (Figure 2) for the manganese binding site 1 within the N-terminal domain (*9*, *17*). By contrast, some have argued for catalysis occurring at site 2 (*8*). However, there is growing evidence for site 1 being the sole or major catalytic site and for the manganese binding site 2 in the C-terminal domain to be purely structural on the basis of mutagenesis and structural studies (*9*, *18*), homology modeling (*19*), kinetic isotope effects with mutant enzymes (*20*), and the reported differential binding of formate to each site according to high-field EPR spectroscopy (*21*). Problems

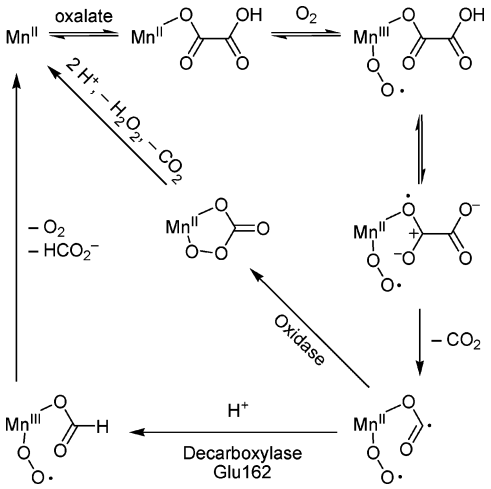

FIGURE 1: Current hypothesis for the divergent catalytic mechanisms of oxalate decarboxylase and oxalate oxidase.

† This work was supported by the Biotechnology and Biological Sciences Research Council with a Biochemistry and Cell Biology Committee studentship (to M.R.B.), a grant (C18140 to V.J.J.), and a Core Strategic Grant to the John Innes Centre.

‡ Data deposition: Atomic coordinates and structure factors have been deposited in the Protein Data Bank, www.pdb.org (PDB ID code 2v09).

* To whom correspondence should be addressed. E-mail: stephen.bornemann@bbsrc.ac.uk. Phone: +44-1603-450741. Fax: +44-1603-450018.

10.1021/bi700947s CCC: $37.00
Published on Web 10/09/2007

```
                                        Lid
B.subtilis          OxdC    155 FDDGSFSENSTFQLTDWL
C.subvermispora     OxoX-G  235 FPDGTFDASNQFMITDWL
C.subvermispora     OxoX-C  231 FPDGTFDSSNQFMITDWL
H.vulgare           OxoX    153 FNSQNP---GIVFVPLTL
```

FIGURE 2: Protein sequences of the lid region of oxalate decarboxylase and oxidases. The protein sequences shown are of oxalate decarboxylase from *B. subtilis* (OxdC GenBank accession no. O34714) and of oxalate oxidases from *Ceriporiopsis subvermispora* (OxoX-G GenBank accession no. AJ563660 and OxoX-C GenBank accession no. AJ746414) and barley (*Hordeum vulgare*) oxalate oxidase (GenBank accession no. P45850). The *H. vulgare* sequence was structurally aligned with the *B. subtilis* OxdC N-terminal domain (*18*). The five amino acids known to form a lid over the manganese binding site 1 of *B. subtilis* OxdC are indicated by the box.

with these studies are that mutations in site 2 have tended to give unstable proteins, precluding their detailed characterization, and proving a lack of activity in site 2 definitively (i.e., a negative) is difficult.

Both the oxidase and the decarboxylase possess small amounts of the other respective activity (*6*, *19*), suggesting the possibility of engineering a reaction specificity switch with either enzyme. Although the substitution of Glu162 in the bacterial decarboxylase was expected to have converted it into an oxidase, this was not the case (*9*). There is a recent report that the E162Q mutant of oxalate decarboxylase exhibits a ~200-fold loss in decarboxylase activity and a ~10-fold increase in oxalate oxidase activity to give a specificity switch of ~2500 (*20*). This provided more support for site 1 being the sole active site, but the magnitude of the switch was moderate. In addition, in our hands, this mutant had a specificity switch of only ~90 (*9*). We recently sequenced a fungal oxidase that was more closely related to the bacterial decarboxylase than any other oxidase (*19*). This provided evidence not only that the loss of Glu162 was crucial, but also that other amino acid substitutions of the lid might be important (Figure 2), even though all but one (Thr165) of their side chains would not be expected to form part of the lining of site 1 on the basis of existing structures. A theoretical study has suggested that the intrinsic reactivity of oxalate decarboxylase site 1 is actually toward oxalate oxidation and that decarboxylation is the consequence of an elaboration of the site through not only the addition of the general acid but also electrostatic changes (*15*). This implies that the lid may be responsible for defining the electrostatic environment of the site. Interestingly, the less closely related plant oxidase has no lid, but deletion of the lid in the decarboxylase does not switch its activity, presumably because of other differences in this more distantly related enzyme (*18*).

This work addresses whether reaction specificity can be controlled by the lid peptide sequence, the number of amino acid substitutions required to maximize such a switch, whether Glu162 is crucial for decarboxylase activity, what role residues other than Glu162 have, which manganese binding sites are catalytically active, and whether radicals can be trapped during catalysis.

EXPERIMENTAL PROCEDURES

Preparation of Mutant Enzymes. Site-specific mutants of *B. subtilis* oxalate decarboxylase OxdC were prepared using the QuikChange kit (Stratagene). Proteins with a C-terminal His tag were expressed in *Escherichia coli*, purified using nickel affinity chromatography, and treated with Chelex 20 resin (Bio-Rad) to remove adventitious metal ions as described previously (*9*), except that the cells were heat-shocked at 42 °C for 18 min (*22*) rather than 2 min prior to induction of protein expression. Protein was determined using the Pierce Coomassie Plus-200 assay using bovine serum albumin as the standard. This method has been shown to be consistent with amino acid analysis (*18*). Metal analysis was provided by Southern Water Scientific Services (Lewes, Sussex, U.K.) using inductively coupled plasma emission spectroscopy of acid-digested samples.

Enzyme Assays. Oxalate decarboxylase activity was measured in stopped assays where the production of formate was determined using an NAD-requiring formate dehydrogenase (*9*). Oxalate oxidase and oxalate-dependent dye oxidation activities were determined in 50 mM succinic acid/NaOH, pH 4.0, with 2,2′-azinobis(3-ethylbenzthiazoline-6-sulfonic acid) with and without horseradish peroxidase as described previously (*9*). The value obtained without peroxidase had to be subtracted from that in its presence to obtain the rate of hydrogen peroxide production. The dissolved dioxygen concentration was determined in 50 mM succinic acid/NaOH, pH 4.0, using a Clark-type (*23*) oxygen electrode (Rank Brothers Ltd.). One unit of enzyme activity was defined as the consumption or production of 1 μmol of substrate or product, respectively/min. Kinetic constants and their standard errors were estimated by fitting data using the Pharmacology Simple Ligand Binding One Site Saturation option in Sigmaplot v8.0 (Systat Software Inc.).

Purification of Plant and Fungal Oxalate Oxidases. Barley (*Hordeum vulgare*) oxalate oxidase was purified from hydroponically grown seedling roots using heat treatment, concanavalin-A affinity, carboxymethyl-Sepharose, and gel filtration chromatographies as described previously (*5*). The G isoform of the fungal (*Ceriporiopsis subvermispora*) enzyme was expressed in *E. coli* as described previously (*19*). It was partially purified by dialysis against 50 mM phosphate buffer, pH 3.0, MonoQ anion exchange (Amersham; with a 0−0.8 M NaCl gradient), Hitrap butyl FF hydrophobic interaction (Amersham; with positive 0−40% ethylene glycol and negative 3−0 M NaCl gradients), reactive green-5 (Sigma; with a 2−100 mM imidazole stepped gradient), and Superdex 200 gel permeation (Amersham) chromatographies.

EPR Spectroscopy. X-band (9 GHz) EPR spectroscopy was performed on a Bruker ELEXSYS 500 spectrometer with an ER049X SuperX microwave bridge, an ER4122SHQE cavity, and an Oxford Instruments ESR-900 cryostat with an ITC3 temperature controller. A buffer-only spectrum was subtracted from each spectrum. Spectra were simulated using Simfonia v1.25 (Bruker). Reaction mixtures (50 μL) for spin trapping were buffered with 50 mM succinic acid/NaOH, pH 4.0, containing 20% glycerol and 200 mM NaCl. Each sample was drawn into a glass capillary after mixing and sealed with Cristaseal putty (Hawksley and Sons Ltd.) before being placed in a plastic Pasteur pipet that was heat-sealed at one end. Manual freeze quenching was carried out by mixing enzyme with substrate in a Perspex T mixing block fitted with a stainless steel needle allowing collection of the sample in an EPR tube before freezing within 5 s of mixing in isopentane cooled to −130 °C with liquid nitrogen. Rapid

freezing was accomplished using an apparatus previously described that allowed the freezing of the rapidly mixed sample directly into cooled isopentane as a "snow" (*24*).

Circular Dichroism Spectropolarimetry. Spectra were obtained using a JASCO J-810 spectropolarimeter at ambient temperature with quartz cuvettes and a 1 cm path length. Control spectra without protein were subtracted from those with protein. Protein solutions were buffered with 50 mM Tris/HCl, pH 8.5, containing 0.5 M NaCl.

Protein Crystallography. Protein was crystallized using the hanging drop vapor diffusion method in VDX plates (Hampton Research) using 1 μL of ~10 mg mL^{-1} protein solution in 50 mM Tris/HCl, pH 8.5, containing 500 mM NaCl mixed with 1 μL of precipitant (4.5% (w/v) PEG 2000 (Fluka) buffered with 100 mM Tris/HCl, pH 8.5, containing 100 mM glycine, 5 mM DTT, and 0.5 mM $MnCl_2$) suspended over 1 mL of precipitant at 18 °C. Crystals were cryoprotected in crystallization solution containing 25% (w/v) glycerol before being flash frozen on a cryoloop (Hampton Research) by plunging into liquid nitrogen. Diffraction data from a single crystal were recorded at 100 K using a Quantum 4 ADSC CCD detector on station PX14.1 (wavelength 1.488 Å) at the Synchrotron Radiation Source, Daresbury, U.K. Images were collected with a 1° oscillation and an exposure time of 60 s. Data were processed using MOSFLM (*25*) and SCALA (*26*), and further downstream processing was effected using programs from the CCP4 suite (*27*). Initial phases were obtained by rigid body refinement of an existing structure (PDB ID 1uw8 (*9*)) using REFMAC5 (*28*). Crystals belonged to space group *R*32 with cell parameters of $a = b = 154.6$ Å and $c = 123.0$ Å (hexagonal setting) and contained a single monomer per asymmetric unit, giving an estimated solvent content of 62% (*29*). Data collection and processing statistics are summarized in Table 1. Model building was performed with the program COOT (*30*) with reference to SIGMAA-weighted (*31*) $2mF_o - DF_c$ and $mF_o - DF_c$ Fourier electron density maps. Positional and thermal parameters of the model were subsequently refined using REFMAC5. A subset of the data comprising a random 5% of the reflections was excluded from refinement and used in the calculation of the "free" (R_{free}) crystallographic *R* factor (*32*). A summary of the model contents and geometrical parameters of the final structure is given in Table 1 (*33*, *34*). The plant oxalate oxidase (PDB ID 1fi2 (*7*)) and a wild-type oxalate decarboxylase structure (1uw8 (*9*) were structurally aligned using Expresso (*35*) as reported earlier (*18*).

Table 1: Summary of X-ray Data and Model Parameters

data collection	
resolution range[a] (Å)	30.19−1.80 (1.90−1.80)
no. of unique reflections	49 648 (5472)
completeness[a] (%)	95.3 (72.8)
redundancy	6.5 (2.0)
R_{merge}[a,b]	0.086 (0.308)
$\langle I\rangle/\langle\sigma(I)\rangle$[a]	15.9 (2.5)
Wilson *B* value (Å^2)	13.7
refinement	
R_{cryst}[c] (based on 95% of the data; %)	14.1
R_{free}[c] (based on 5% of the data; %)	17.3
DPI[d] (based on R_{free}; Å)	0.085
no. of residues with most favored Φ/Ψ[e] (%)	89.8
RMSD(bond distances) (Å)	0.018
RMSD(bond angles) (deg)	1.660
contents of model (no. of molecules/no. of non-hydrogen atoms)	
protein (no. of residues/no. of atoms)	377/2974
manganese ions	2
waters	471
Tris	1/8
average temperature factors (Å^2)	
main chain atoms	11.6
side chain atoms	13.8
manganese ions	10.0
waters	25.5
Tris	16.3
overall	14.4

[a] The figures in parentheses indicate the values for the outer resolution shell. [b] $R_{merge} = \sum_h\sum_l|I_{hl} - \langle I_h\rangle|/\sum_h\sum_l\langle I_h\rangle$, where I_l is the *l*th observation of reflection *h* and $\langle I_h\rangle$ is the weighted average intensity for all observations *l* of reflection *h*. [c] The *R* factors R_{cryst} and R_{free} are calculated as follows: $R = \sum(|F_o - F_c|)/\sum|F_o| \times 100$, where F_o and F_c are the observed and calculated structure factor amplitudes, respectively. [d] Diffraction-component precision index (*34*); an estimate of the overall coordinate errors calculated in REFMAC5 (*28*). [e] As calculated using PROCHECK (*33*).

RESULTS AND DISCUSSION

Oxalate Decarboxylase and Oxidase Activities of Oxalate Decarboxylase Lid Mutants. A series of *B. subtilis* OxdC oxalate decarboxylase mutants were constructed to test the dependence of reaction specificity on the site 1 lid amino acid sequence. The substitutions chosen were initially guided by the lid sequence of the G isoform of the *C. subvermispora* fungal oxalate oxidase (*19*). Oxalate decarboxylase and oxidase activities were determined by measuring the production of formate in a stopped assay and by monitoring the production of hydrogen peroxide in real time using a linked assay involving a dye together with a peroxidase, respectively. The substitution of the first two of the five amino acids of the lid with SE161-2DA led to a dramatic lowering of decarboxylase activity to <1% compared with the wild-type activity (Table 2), as would be expected with the loss of Glu162. This was accompanied by a 9.6- and 8.1-fold increase in oxalate oxidase V_{max} and k_{cat}/K_m, respectively (Table 3), which is comparable to observations made by others with the E162Q mutant (*20*). However, oxidase activity in both cases remained low in absolute terms. The additional substitution of the third amino acid with SEN161-3DAS gave decarboxylase activity at the limit of detection and a further significant increase in oxidase V_{max} and k_{cat}/K_m to 30 and 31 times that of the wild type, respectively. By taking a ratio, for the wild-type and SEN161-3DAS enzymes, of the ratios of the V_{max} for each activity, a specificity switch of 282 000 can be calculated.

To establish the influence of other residues of the lid, an ENS162-4ASN mutant was also tested. The decarboxylase activity was again <1% (Table 2). Although the oxidase V_{max} remained as high as with the SEN161-3DAS mutant, at 34-fold higher than that of the wild type, the K_m for oxalate was compromised to give a k_{cat}/K_m only 1.4-fold higher than that with the wild-type enzyme (Table 3), making this trisubstituted mutant less effective than the previous one. Making the fourth substitution to give the SENS161-4DASN mutant again led to undetectable decarboxylase activity and the most dramatic increase in oxidase V_{max} to 119-fold higher than that for the wild type, giving a specificity switch of 225 000. Again, the K_m for oxalate was compromised, but the k_{cat}/K_m was still 6.2-fold higher than that for the wild type.

Table 2: Oxalate Decarboxylase Activity of Oxalate Decarboxylase Lid Mutants

mutant	V_{max}[a] (U mg^{-1})	$K_m^{oxalate}$ (mM)	k_{cat}/K_m[a] (M^{-1} s^{-1})	Mn content (no. of atoms/subunit)
wild type	94.9 ± 2.3 (100)	6.6 ± 0.6	10 670 ± 960 (100)	1.2
SE161-2DA	0.36 ± 0.01 (0.4)	9.1 ± 1.1	29 ± 4 (0.3)	1.2
SEN161-3DAS	<0.01[b] (<0.01)	*c*	*c*	1.4
ENS162-4ASN	0.50 ± 0.01 (1)	2.0 ± 0.2	185 ± 20 (2)	1.3
S161D/NS163-4SN	37 ± 1 (39)	97 ± 7	290 ± 20 (3)	1.4
SENS161-4DASN	0.05[b] (0.05)	*c*	*c*	1.6
SENS161-4DSSN	0.04[b] (0.04)	*c*	*c*	1.4
SENST161-5DASNQ	0.01[b] (0.01)	*c*	*c*	1.2

[a] Expressed as formate production. Values in parentheses indicate the percentage compared with the value for the wild-type enzyme. [b] The specific activity of low-activity mutants was determined directly from a standard assay. [c] Not determined.

Table 3: Oxalate Oxidase Activity of Oxalate Decarboxylase Lid Mutants and Oxalate Oxidases from *C. subvermispora* and *H. vulgare*

mutant	V_{max}[a] (U mg^{-1})	$K_m^{oxalate}$ (mM)	k_{cat}/K_m[a] (M^{-1} s^{-1})	specificity switch[b]
wild type	0.038 ± 0.003 (1)	0.27 ± 0.11	105 ± 46 (1)	1
SE161-2DA	0.36 ± 0.01 (9.6)	0.31 ± 0.04	870 ± 120 (8.1)	2500
SEN161-3DAS	1.13 ± 0.03 (30)	0.26 ± 0.03	3250 ± 350 (31)	282 000
ENS162-4ASN	1.31 ± 0.05 (34)	6.4 ± 0.6	152 ± 15 (1.4)	6500
S161D/NS163-4SN	0.13 ± 0.02 (3.3)	12 ± 4	8 ± 3 (0.07)	9 (25 600[c])
SENS161-4DASN	4.5 ± 0.2 (119)	5.3 ± 0.5	630 ± 60 (6.2)	225 000
SENS161-4DSSN	4.4 ± 0.1 (116)	3.2 ± 0.2	1030 ± 80 (10)	275 000
SENST161-5DASNQ	0.19 ± 0.01 (5.1)	0.87 ± 0.23	166 ± 45 (1.6)	47 000
C. subvermispora oxidase[d]	19.5 ± 0.7	0.55 ± 0.08	38 700 ± 5500	*e*
H. vulgare (barley) oxidase	16.8 ± 0.8	1.1 ± 0.2	5400 ± 200	*e*

[a] Expressed as hydrogen peroxide production. Values in parentheses indicate the fold increase compared with the value for the wild-type decarboxylase enzyme. [b] Specificity switch defined as the ratio of ratios of oxidase and decarboxylase activities between a mutant and the wild type. [c] Specificity switch using the SENS161-4DASN mutant as the reference rather than the wild type. [d] Partially purified; see the Results and Discussion. [e] Not applicable.

To test the influence of the lid sequence of the other C isoform of the fungal oxidase, a SENS161-4DSSN mutant was constructed. The properties of this mutant were very similar to those of the G-isoform-type mutant SENS161-4DASN, indicating that reaction specificity is somewhat insensitive to the nature of the substitution of Glu162. Substituting all five lid amino acids with the G-isoform-like SENST161-5DASNQ mutant gave undetectable decarboxylase activity again, but the oxidase activity was surprisingly low with a V_{max} and k_{cat}/K_m only 5.1- and 1.6-fold higher than those of the wild type. It is possible that, in the context of the global decarboxylase structure, it is important to allow a hydrogen-bonding interaction in the closed form between Thr165 and Arg92, a critical residue in binding and stabilizing catalytic intermediates (*9*, *18*).

The pivotal test as to whether Glu162 is indeed mainly responsible for reaction specificity was carried out by replacing the Glu162 residue in the SENS161-4DASN mutant that had the highest oxidase V_{max} to give the S161D/NS163-4SN mutant. Remarkably, 39% of the decarboxylase V_{max} of the wild type was recovered (Table 2), while the oxidase V_{max} collapsed to only 3.3-fold that of the wild-type enzyme (Table 3), to give a specificity switch of 25 600 relative to the SENS161-4DASN mutant and only 9 relative to the wild-type enzyme. Although the K_m for oxalate in this triple mutant was elevated in both reactions, this result clearly demonstrated that the catalytic outcome is defined primarily by the presence or absence of Glu162.

Comparison with Plant and Fungal Oxalate Oxidases. A partially purified preparation (~40% pure according to a Coomassie-stained denaturing gel) of the recombinant G isoform of the fungal oxidase gave an (under)estimate of V_{max} of 19.5 ± 0.7 U mg^{-1} (consistent with published specific activities of 20 U mg^{-1} for the partially purified recombinant protein (*19*) and 10.4 U mg^{-1} for the protein purified from the fungus (*36*)) and a K_m of 0.55 ± 0.08 mM (the same order of magnitude as a published value of 0.1 mM for the protein purified from the fungus (*36*)) (Table 3).

The mutant with the highest oxidase V_{max} was SENS161-4DASN at 4.5 ± 0.2 U mg^{-1}, which was clearly lower than that of the partially purified recombinant fungal oxidase (Table 3). The mutant with the highest k_{cat}/K_m, SEN161-3DAS, had an oxalate K_m value for the oxidase reaction (0.26 ± 0.03 mM) of the same order of magnitude as the fungal enzyme (0.55 ± 0.08 mM) and the wild-type enzyme (0.27 ± 0.11 mM). Therefore, it was possible to engineer substantial oxidase activity into the wild-type decarboxylase without compromising the K_m for oxalate. Nevertheless, the k_{cat}/K_m of the SEN161-3DAS mutant (3250 ± 350 M^{-1} s^{-1}) was significantly lower than for the fungal oxidase (38 700 ± 5500 M^{-1} s^{-1}). These results again indicate the influence of the context of the lid within the global protein structure.

For an additional comparison, the plant enzyme was purified to homogeneity from barley (*H. vulgare*). Although its V_{max} (16.8 ± 0.8 U mg^{-1}) was higher than that for any of the mutants, its k_{cat}/K_m with air-saturated buffers (5400 ± 200 M^{-1} s^{-1}) was of the same order of magnitude as that of the most efficient mutant (SEN161-3DAS at 3250 ± 350 M^{-1} s^{-1}; Table 3).

Manganese Content and Environment in the Mutant Enzymes. Metal analysis showed that there was a small degree of variability in the manganese content between each mutant enzyme (Table 2). There was no correlation between metal content and reaction specificity.

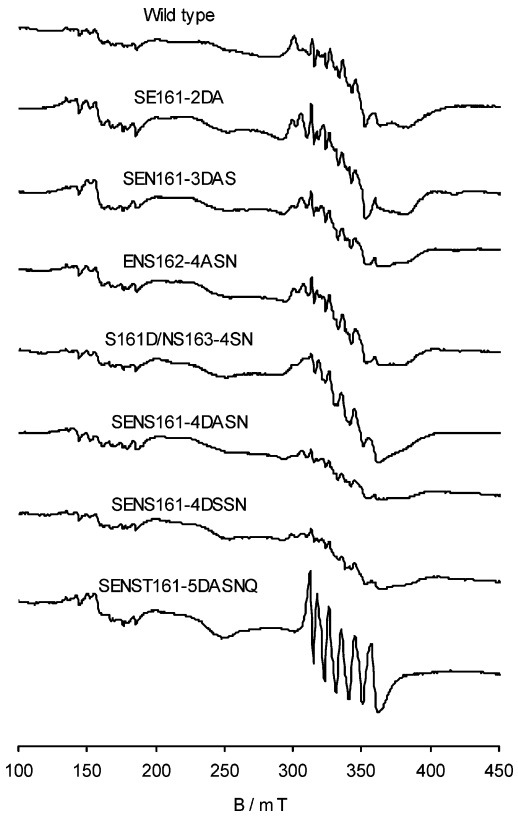

FIGURE 3: X-band EPR spectra of oxalate decarboxylase wild-type and lid mutant enzymes. Samples contained 224 μM enzyme, 50 mM Tris/HCl, pH 8.5, and 500 mM NaCl. The signal amplitudes were adjusted to take into account the manganese content of each mutant (Table 2). Spectra were recorded at 30 K with a microwave power of 1 mW.

The electronic environment of the manganese binding sites in the mutants was investigated using X-band EPR spectroscopy (Figure 3). The wild-type enzyme is known to give a $g \approx 2$ six-line ^{55}Mn ($I = 5/2$) multiplet nuclear hyperfine split signal ($a^{Mn} = 9.5$ mT) (*6*). In the current study we prepared samples in the presence of noninhibitory concentrations of NaCl. Wild-type protein spectra exhibited an increased line width of the main manganese(II) signal and the appearance of broad features over a wide field range consistent with the reported effect of chloride ions on recombinant barley oxalate oxidase (*37*).

We noted a general correlation between the number of amino acid substitutions and an increase in broadening (reduction of the resolution) of the main manganese(II) hyperfine structure. Such broadening would be associated with decreased electronic isotropy and a more distorted octahedral environment. This was most apparent in the tetrasubstituted mutants with the highest oxidase V_{max} values. There are of course two manganese binding sites in each enzyme, but a recent high-field EPR study of the wild-type enzyme by Angerhofer et al. (*21*) has established that site 2 (which they refer to as site I) has greater zero-field splitting, and therefore a much broader signal, than site 1. The substantial broadening of the spectral features shown in Figure 3 would therefore be expected to largely reflect changes in the site 1 manganese environment associated with the mutations of the site 1 lid. Quantification and simulation of such overlapping manganese EPR signals in the X-band has proven to be too challenging to give meaningful information. The exception to the trend between the number of mutations and line broadening was the relatively inactive pentasubstituted enzyme that showed a dramatic sharpening and simplification of the hyperfine multiplet indicative of increased electronic isotropy and of a less distorted octahedral environment. This would most probably be associated with site 1, but a contribution from site 2 cannot be excluded. The half-field signal centered around $g \approx 4.3$ (~160 mT) that was present in all of the spectra was most probably associated with the moderate zero-field splitting of the main $g \approx 2$ signal, as has been suggested recently (*12*).

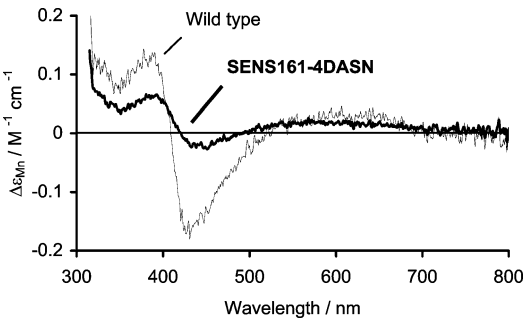

FIGURE 4: Circular dichroism spectra of the as-isolated wild-type (narrow line; 0.54 mM protein, 0.65 mM Mn) and SENS161-4DASN mutant (broad line; 0.90 mM protein, 1.44 mM Mn) enzymes.

Circular dichroism spectroscopy of the wild-type enzyme and the SENS161-4DASN mutant gave spectra (Figure 4) that were very similar to that obtained with the recombinant plant oxalate oxidase after treatment with periodate and ascorbate (*38*). These features are weak, but characteristic of Mn(III) and particularly useful because no Mn(III) EPR signals have been identified with oxalate-degrading enzymes at the X- and W-bands with as-isolated enzymes and at the X-band during turnover presumably because of unfavorable zero-field splitting parameters and the presence of strong Mn(II) signals (*5*, *6*, *12*, *21*, *37*, *38*; see also below). The magnitude of the circular dichroism feature at ~390 nm indicated that about 15% of the Mn in the wild-type enzyme was in the Mn(III) oxidation state. It is clear that the proportion of Mn(III) in the mutant enzyme was about half of that in the wild type.

Structure of the SENS161-4DSSN Mutant. We obtained a crystal structure of the SENS161-4DSSN mutant to 1.8 Å resolution, which had full occupancy of manganese ions. A summary of the data and model parameters is shown in Table 1. It was clear that the overall fold of the protein was unchanged, giving an rmsd from the closed wild-type decarboxylase structure of 0.25 Å. The only significant deviation between the two structures was the conformation of the lid itself, being between the open (*8*) and closed (*9*) forms of the wild-type decarboxylase enzyme (Figure 5). However, there was some evidence of disorder in the lid (average main chain temperature factor of 20.6 Å^2 for residues 161−165 as compared to the overall main chain value of 11.6 Å^2). There was no formate bound to the site 1 manganese, like with the closed structure, but unlike the open form of the wild-type enzyme. The loss of the Glu162 side chain resulted in a water molecule occupying the position that the carboxyl group occupied in the closed structure. Importantly, the structure of the site 2 manganese site appeared to be unchanged compared with that of the wild-type decarboxylase (not shown).

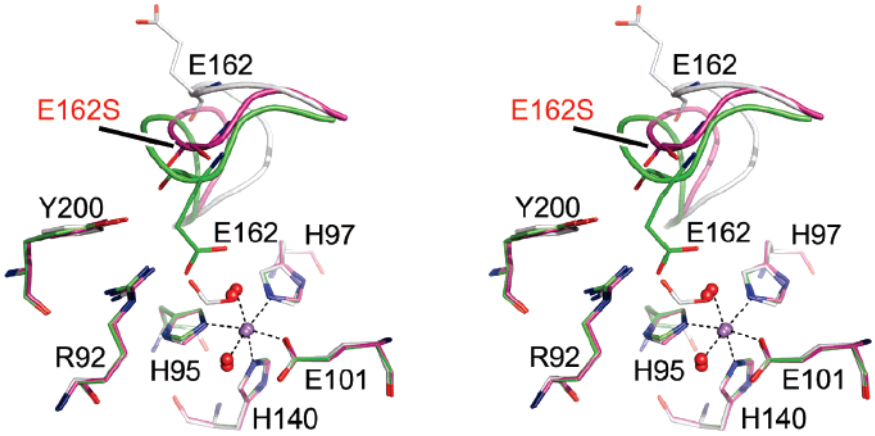

FIGURE 5: Wall-eyed stereoview showing key residues and ligands around site 1 and the lid region. The SENS161-4DSSN mutant structure is depicted with magenta carbons. The wild-type open (PDB code 1J58 (*8*)) and closed (PDB code 1UW8 (*9*)) structures are shown for reference with carbons colored gray and green, respectively. The main chain backbone of the lid regions (residues 160−166) is shown in ribbon representation, with residue 162 shown in full atom representation in each case. The dotted lines indicate interactions between the manganese, its protein ligands, and water molecules in the closed structure. Site 2 was not affected (not shown). The figure was generated using PyMOL (http://www.pymol.org).

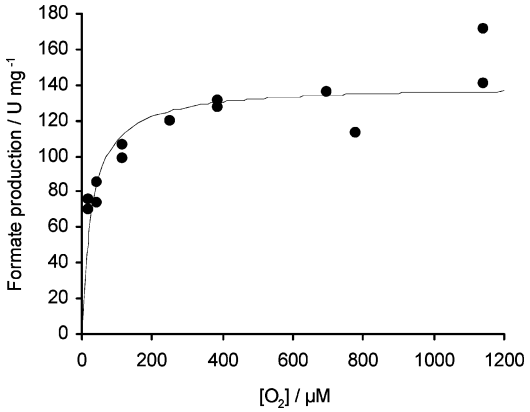

FIGURE 6: Dioxygen dependence of the wild-type oxalate decarboxylase reaction. Formate production was determined using the adapted stopped assay after 30 s of reaction within the cell of a Clark-type electrode. Reaction mixtures contained 0.4 μM enzyme, 150 mM oxalate, 100 mM citrate/HCl, pH 4.0, 300 μM 1,2-diaminobenzene, and 10 μg mL^{-1} bovine serum albumin. The dissolved dioxygen concentration was defined by mixing nitrogen-, air-, and dioxygen-saturated buffers. The smooth line represents a best fit using the Michaelis−Menten equation with K_m = 28 ± 8 μM and V_{max} = 140 ± 7 U mg^{-1}.

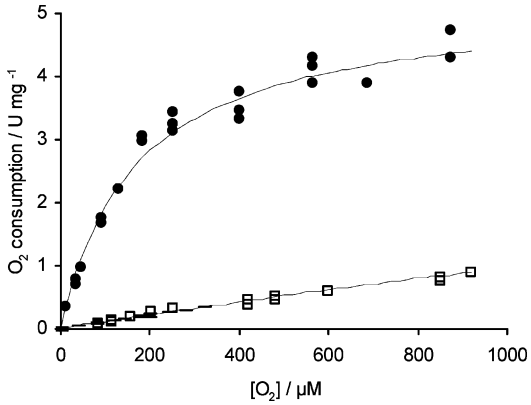

FIGURE 7: Dioxygen dependence of the SENS161-4DASN mutant (●) and wild-type oxalate decarboxylase (□) enzymes with respect to oxalate oxidase activity. Reaction mixtures contained 20 mM oxalate in 50 mM succinic acid/NaOH, pH 4.0. The dissolved dioxygen concentration was measured using a Clark-type oxygen electrode. The initial dissolved dioxygen concentration was defined by mixing nitrogen-, air-, and dioxygen-saturated buffers. The smooth lines represent best fits using the Michaelis−Menten equation, giving K_m = 168 ± 14 μM and V_{max} = 5.25 ± 0.15 U mg^{-1} for the mutant and K_m = 4.8 ± 2.4 mM and V_{max} = 5.6 ± 2.4 U mg^{-1} for the wild type.

Dependence of Catalysis on Dioxygen. Decarboxylase activity was determined as a function of dissolved dioxygen concentration using a 30 s stopped assay (Figure 6). This gave a K_m for dioxygen of 28 ± 8 μM and a V_{max} of 140 ± 7 U mg^{-1}. Since air-saturated buffers at 23 °C contain about 260 μM dissolved dioxygen (*23*), it was clear that the enzyme was capable of working close to its maximum rate in such a buffer. This bacterial enzyme has been detected in the cytoplasm (*4*) and somewhat unexpectedly in the cell wall (*39*), so whether the dissolved dioxygen concentration would ever be this high in these locations is an interesting issue not addressed here. Turnover-dependent denaturation of the enzyme was observed at reaction times >2 min with >350 μM dioxygen, similar to that observed previously with the *Aspergillus niger* oxalate decarboxylase (*11*, *40*).

The dependence on dioxygen of the oxalate oxidase reaction was determined for a mutant with a high oxidase activity and compared with that of the wild-type enzyme (Figure 7). The SENS161-4DASN mutant exhibited a K_m for dioxygen of 168 ± 14 μM and a V_{max} of 5.25 ± 0.15 U mg^{-1}. The oxidase activity of the wild-type enzyme was not even close to reaching saturation up to a dissolved dioxygen concentration of 920 μM. This showed that the K_m for dioxygen of the wild-type decarboxylase in its minor oxidase activity was extremely high and somewhat remarkably several orders of magnitude higher than that for its normal decarboxylase reaction (noting that $K_m \neq K_d$). It would therefore appear that the lid sequence does indeed have an influence over the dioxygen saturation behaviors with each of the two reactions and that this is a factor, at least in part, in the control of reaction specificity.

When the experiment was carried out with the purified wild-type plant oxalate oxidase, the K_m for dioxygen was 430 ± 70 μM and the V_{max} was 159 ± 10 U mg^{-1}, giving a k_{cat}/K_m (for dioxygen) of 130 000 ± 23 000 M^{-1} s^{-1}. For comparison, a commercial (Boehringer Mannheim) partially purified preparation gave an indistinguishable K_m of 480 ± 110 μM. Surprisingly, it was clear that the plant enzyme

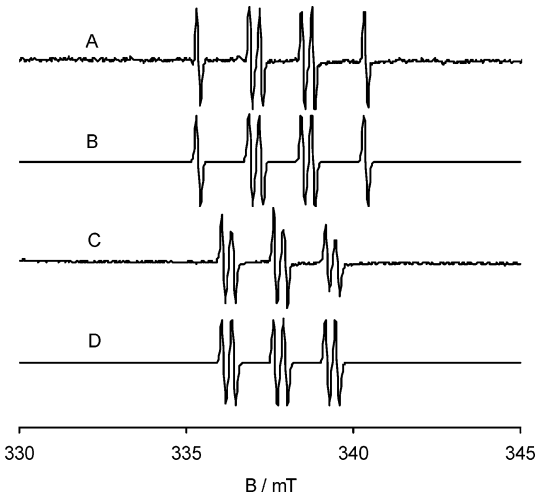

FIGURE 8: X-band EPR of spin-trapped free radicals produced by the SENS161-4DASN mutant: (A) spectrum obtained in the presence of 5,5-dimethyl-1-pyrroline *N*-oxide (average of eight scans), (B) simulation of spectrum A with nuclear hyperfine coupling constants of $a^N = 1.57$ mT and $a^H = 1.87$ mT, (C) spectrum obtained in the presence of *N-tert*-butyl-α-(4-pyridyl)-nitrone *N*′-oxide (average of 36 scans), (D) simulation of spectrum C with nuclear hyperfine coupling constants of $a^N = 1.55$ mT and $a^H = 0.28$ mT. Reaction mixtures contained 27 μM enzyme, 100 mM oxalate, and 50 mM spin trap. Experimental spectra were recorded at 298 K with a microwave power of 5 mW. The first scan was taken within 2 min, and each scan took <2 min.

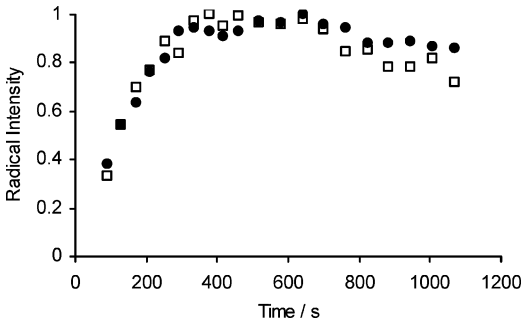

FIGURE 9: Time courses of normalized spin-trapped free radical adduct formation with the SENS161-4DASN mutant. The yield of spin-trapped radical was determined by double integration of the signals obtained in the presence of either 5,5-dimethyl-1-pyrroline *N*-oxide (●) or *N-tert*-butyl-α-(4-pyridyl)nitrone *N*′-oxide (□), each at 50 mM, at various incubation times. Single scans of narrow field width were taken with 40−60 s intervals.

could not operate at maximal rates in air-saturated buffers. However, in a photosynthesizing leaf tissue (*41*), but not in nonphotosynthetic root tissue (*42*), the dissolved dioxygen concentration can be significantly higher. Interestingly, the K_m for dioxygen of the plant oxidase was of the same order of magnitude as that with the SENS161-4DASN mutant.

Oxalate-Dependent Free Radical Species. During turnover of the SENS161-4DASN mutant enzyme, a free radical was trapped in the presence of 5,5-dimethyl-1-pyrroline *N*-oxide (commonly known as DMPO) (Figure 8). This gave a six-line spectrum at $g = 2.006$. No signal was observed in the absence of either enzyme, oxalate, or the spin trap. A simulation of the spectrum gave nuclear hyperfine coupling constants consistent with literature values for a carboxylate radical adduct (*43*). This assignment was supported by repeating the experiment with *N-tert*-butyl-α-(4-pyridyl)-nitrone *N*′-oxide (commonly known as POBN; Figure 8) to give a signal centered around $g = 2.006$ with the expected (*43*) coupling constants. There was no indication of the trapping of other radicals such as superoxide with either radical trap.

Time courses of the signal intensities showed that they formed steadily up to about 400−500 s to reach a plateau and then decayed a little (Figure 9). Although carboxylate radicals are known to react with dioxygen, the high concentration of the spin trap (50 mM) would have ensured efficient trapping. The decay of the signal at longer times would be expected because the spin adduct with DMPO, for example, is known to decay at low pH due to protonation (*44*). In the conditions used, it was expected that the enzyme would turn over in a period of ∼500 s, indicating that the carboxylate radical was being formed during turnover.

The wild-type enzyme, on the other hand, gave no signal with 5,5-dimethyl-1-pyrroline *N*-oxide but did give a small signal with *N-tert*-butyl-α-(4-pyridyl)nitrone *N*′-oxide (data not shown) which was 4.4-fold lower in intensity than that formed with the mutant in Figure 8. This is the first time this radical has been detected with an oxalate decarboxylase enzyme. Its low signal intensity with the wild type precluded a time course to be obtained with confidence. Although a carboxylate radical has been observed with the recombinant barley oxalate oxidase, in this case it was established that it was not associated with turnover (*37*). We have obtained new evidence that oxalate decarboxylase is capable of radical chemistry with oxalate and, for the mutant enzyme at least, that it occurs during turnover. Quantification of spin-trapped radicals is difficult, and carboxylate radicals have not been observed in freeze quench experiments (see below) presumably because these reactive species do not accumulate sufficiently. Whether the carboxylate radical is kinetically competent or a side product will need to be established.

The wild-type oxalate decarboxylase is known to generate a Tyr radical during turnover in an off-catalytic cycle pathway at pH 5.2 (*12*). It has been suggested that it forms either to facilitate coupling between the two manganese binding sites or more likely to quench any reactive off-catalytic pathway radical intermediates. It was possible to observe this species using rapid freeze EPR with the SENS161-4DASN mutant (Figure 10 in the Supporting Information) with no evidence for additional signals, such as Mn(III), in either perpendicular or parallel EPR modes. The signal at $g = 2.002$ with a peak to trough width of ∼2.1 mT was observed 0.1 s after mixing but decayed 2 s after mixing. The same signal was also observed with the wild type near its pH optimum (*17*, *22*) at pH 4.0 (Figure 11 in the Supporting Information).

Oxalate-Dependent Dye Oxidation Activity of Mutant Enzymes. Oxalate decarboxylases and oxidases are known to catalyze an oxalate-dependent dye oxidation reaction at typically <1% and <10% the rate of their main reactions, respectively (*6*, *19*). The mutant enzymes also catalyzed this side reaction (Table 4). The V_{max} values for this reaction were strongly linearly correlated with those for the oxalate oxidase reaction ($r^2 = 0.969$; Figure 12 in the Supporting Information), but their k_{cat}/K_m values were less so correlated ($r^2 = 0.764$). Thus, the ratio of hydrogen peroxide production to single-electron 2,2′-azinobis(3-ethylbenzthiazoline-6-sulfonic acid) oxidation was 1.3:1 and therefore close to unity. This indicated that the enzyme intriguingly catalyzed about one

Table 4: Oxalate-Dependent Dye Oxidation Activity of Oxalate Decarboxylase Lid Mutants

mutant	V_{max}[a] (U mg^{-1})	$K_m^{oxalate}$ (mM)	k_{cat}/K_m[a] (M^{-1} s^{-1})
wild type	0.49 ± 0.02 (1)	1.0 ± 0.2	370 ± 60 (1)
SE161-2DA	1.20 ± 0.03 (2.4)	0.19 ± 0.02	4700 ± 500 (13)
SEN161-3DAS	1.41 ± 0.04 (2.9)	0.18 ± 0.02	5900 ± 800 (16)
ENS162-4ASN	1.93 ± 0.04 (3.9)	5.7 ± 0.3	250 ± 20 (0.7)
S161D/NS163-4SN	0.22 ± 0.02 (0.4)	3.7 ± 1.5	44 ± 19 (0.1)
SENS161-4DASN	4.2 ± 0.2 (8.5)	2.7 ± 0.4	1100 ± 200 (3.1)
SENS161-4DSSN	4.4 ± 0.1 (8.9)	3.4 ± 0.2	940 ± 50 (2.6)
SENST161-5DASNQ	0.20 ± 0.02 (0.4)	0.2 ± 0.1	730 ± 500 (2.0)

[a] Expressed as the production of single-electron-oxidized 2,2′-azinobis(3-ethylbenzthiazoline-6-sulfonic acid). Values in parentheses indicate the fold increase compared with the value for the wild-type enzyme.

cycle of normal oxalate oxidation for every cycle of single-electron dye oxidation when in the presence of the dye and implied the coupling of these cycles through a complex among the enzyme, oxalate, and dye.

The dependence on the dye oxidation reaction on the dye concentration was determined spectrophotometrically with the SENS161-4DASN mutant enzyme, giving saturation kinetics with a K_m for the dye of 0.29 ± 0.04 mM (Figure 13 in the Supporting Information). This result strongly suggested that the dye did indeed interact directly with the enzyme and intercept a catalytic intermediate, rather than with some redox-active side product released into solution.

The presence of this dye at a saturating concentration inhibited the normal oxalate oxidase reaction by ~50%, as determined by hydrogen peroxide formation in a 5 min stopped assay, but dioxygen consumption was stimulated somewhat, indicating that the oxidation of the dye was dioxygen-dependent. The inhibition of hydrogen peroxide formation lent further support that the dye was intercepting an on-enzyme catalytic intermediate and showed that the oxalate oxidase activities shown in Table 3 are most likely underestimates because the real-time coupled assay involved the use of this dye. In addition, no evidence for formate as a byproduct was observed using [^{13}C]oxalate and NMR spectroscopy. One can speculate that these results imply that the enzyme was catalyzing the single-electron oxidation of the dye with concomitant reduction of dioxygen to superoxide. This reaction requires oxalate, but it may not be consumed. Clearly, further analysis of the chemistry involved in dye oxidation is required. Although dye oxidation may not have any biological significance, it does provide further evidence for free radical chemistry catalyzed by these enzymes.

CONCLUSIONS

We have demonstrated that it is possible to convert an oxalate decarboxylase into an efficient oxalate oxidase by making between three and four amino acid substitutions in a lid of the site 1 manganese binding site without affecting the structure of site 2. It was possible to revert a mutant enzyme with oxidase activity back to a decarboxylase with only a single amino acid substitution, the reintroduction of a Glu residue at position 162. None of the mutants tested exhibited high levels of both reactions. This gave striking evidence for both the role of Glu162 in the decarboxylase reaction and the central importance of this residue is determining reaction specificity. This is consistent with it acting as the general acid in the decarboxylase reaction. In addition, the magnitude of the specificity switch is such that it is difficult to conceive of site 2 possessing significant activity. Thus, our observations provide the most compelling evidence yet that catalysis occurs only at the site 1 manganese binding site, ending any controversy. Examples of how the specificity for one reaction can be changed into that for another with a single mutation are rare (*45*, *46*). What makes our observations with the oxalate-degrading enzymes, to our knowledge, unique is that a single substrate can be converted so efficiently to different products by changing just one amino acid side chain.

The original hypothesis was that the outcome of catalysis would be dictated solely by the presence of a general acid that promoted the decarboxylase reaction in what was otherwise a similar active site (*6*). However, it is clear that amino acids of the lid other than Glu162 also have a role. Ser161 and Asn163 of the lid together suppress intrinsic oxalate oxidase reactivity within the context of the decarboxylase protein (whether Glu162 is present or absent) but do not suppress decarboxylase activity when Glu162 is present. In other words, the S161D and N163S mutations together appear to create a less restrictive electrostatic environment that allows either oxalate oxidation or decarboxylation to occur, depending on the presence of Glu162. A theoretical study concluded that the intrinsic reactivity of the decarboxylase is toward oxalate oxidation and that electrostatic contributions were also important in defining decarboxylase activity (*15*). It therefore follows that the amino acid side chains of the lid appear to refine the electrostatic environment and reactivity of the active site within the context of the rest of the protein.

We have obtained experimental evidence that the control of reaction specificity by the lid is at least in part dictated by the differential dependence of each reaction on dioxygen. The simplest underlying explanation for this is that it is a consequence of the electrostatic effects of the mutations on the active site (*47*). However, the very different dioxygen saturation behaviors in the decarboxylase and oxidase reactions of the wild-type and mutant enzymes imply more complexity. One can speculate that the binding of dioxygen could follow a different path in the wild-type oxidase side reaction because the normal oxidase path is suppressed. Different paths could involve promotion/avoidance of the protonation of dioxygen-derived catalytic intermediates, differential binding modes to the manganese, or discrete subsites near the manganese center that could transiently bind dioxygen. How different paths could be committed to different catalytic outcomes is not yet clear, except that the protonation of dioxygen-derived intermediates is likely to promote oxidation (*15*). There is no spectroscopic or structural evidence to date for dioxygen being enzyme-bound. A theoretical study on an oxalate oxidase model has indicated that dioxygen may not actually form a stable complex with the manganese site before its reduction and the cleavage of the oxalate C−C bond (*16*). In addition, a theoretical study with an oxalate decarboxylase model has suggested that a formal Mn(III) intermediate may not necessarily exist (*15*). These studies further emphasize the need to better understand exactly how dioxygen participates in both of these reactions.

It has been suggested that the catalytic mechanism of the plant oxalate oxidase involves the insertion of a manganese-bound superoxide radical directly into a manganese-bound oxalate molecule prior to oxalate decarboxylation (*10*). Such a mechanism would be committed to oxalate oxidation and could contribute to the different dioxygen saturation behaviors discussed above. On the other hand, there is electrochemical precedence for the facile decarboxylation of oxalate radicals (*48*). Furthermore, carboxylate radicals were trapped during turnover of the mutant enzyme with oxidase activity (although they have yet to be shown to be kinetically competent). Therefore, the divergent mechanism shown in Figure 1 would appear at this stage to be more consistent with the ability to interconvert these two activities.

There is a recent report presenting evidence that the activity of the plant oxidase is directly proportional to its initial manganese(III) content (*38*). This implies a catalytic cycle based on Mn(III) despite the enzyme being predominantly in the manganese(II) oxidation state as isolated (*5*, *37*). Although many of the steps in such a mechanism for oxalate oxidation have chemical precedence (*5*), it is difficult to conceive of a mechanism for oxalate decarboxylation that requires both manganese(III) and dioxygen (*6*). The implication is that reaction specificity could be controlled by the oxidation state of the enzyme as well as the presence or absence of a general acid and the subsequent saturation behavior with dioxygen. However, circular dichroism spectropolarimetry showed that a mutant enzyme with high oxalate oxidase activity had proportionately less Mn(III) than the wild-type decarboxylase. Therefore, a switch in the oxidation state of the Mn ion appears not to be a factor in reaction specificity, at least in this system.

Another feature of the lid is its ability to gate access to the active site and to control appropriate proton transfers in at least the decarboxylase reaction. Such lid dynamics are likely to have an important influence on the K_m and V_{max} of the reaction if they occur on the same time scale as the overall catalytic cycle. Indeed, the disruption of hydrogen bonds associated with the lid in the open conformation only substantially lowers V_{max} (*18*). Dynamic simulations of the wild-type and mutant lids would allow such affects to be assessed.

We have demonstrated the extreme potential plasticity of oxalate-degrading enzymes, with a single amino acid being capable of dictating reaction specificity. It is perhaps no coincidence that the wild-type enzyme requires three to four amino acid substitutions to enable it to become an efficient hydrogen peroxide-producing enzyme. This is because it is a cytosolic enzyme and such a conversion would be potentially lethal. This begs the question as to which activity came first. There is now both theoretical and experimental evidence that the decarboxylase reaction is an elaboration of the oxidase reaction. The oxidases are thought to be exclusively extracellular and can be either monocupins (*1*) or bicupins (*36*), while the decarboxylases appear to be either intracellular (*4*) or extracellular (*49*) and exclusively bicupins (*2*). Therefore, perhaps an extracellular monocupin oxidase gave rise to a bicupin variant, which subsequently became a bicupin decarboxylase that finally lost its secretion signal. One can speculate further that the initial oxalate oxidase evolved from another enzyme involved in stress responses, an extracellular monocupin manganese-dependent superoxide dismutase, several examples of which have been identified in recent years (see ref *50* and references therein).

ACKNOWLEDGMENT

We thank Sascha Keller for assistance with crystallographic data collection, Myles Cheesman from the Centre for Metalloprotein Spectroscopy and Biology at the University of East Anglia for recording the circular dichroism spectra, David J. Lowe for help with the rapid freeze quench experiments, Nigel Richards for helpful discussions, and a reviewer who suggested the interesting possibility of subsites for dioxygen binding.

SUPPORTING INFORMATION AVAILABLE

Figures 10 and 11 showing freeze-quench EPR spectra for the SENS161-4DASN mutant and wild-type enzymes, Figure 12 showing a correlation between the V_{max} values for oxalate oxidation and oxalate-dependent single-electron dye oxidation, and Figure 13 showing the dye dependence of the SENS161-4DASN oxalate-dependent single-electron dye oxidation reaction. This material is available free of charge via the Internet at http://pubs.acs.org.

REFERENCES

1. Dunwell, J. M. (1998) Cupins: A new superfamily of functionally diverse proteins that include germins and plant storage proteins, *Biotechnol. Genet. Eng. Rev. 15*, 1−32.
2. Dunwell, J. M., Khuri, S., and Gane, P. J. (2000) Microbial relatives of the seed storage proteins of higher plants: conservation of structure and diversification of function during evolution of the cupin superfamily, *Microbiol. Mol. Biol. Rev. 64*, 153−179.
3. Dunwell, J. M., Purvis, A., and Khuri, S. (2004) Cupins: the most functionally diverse protein superfamily? *Phytochemistry 65*, 7−17.
4. Tanner, A., and Bornemann, S. (2000) *Bacillus subtilis* YvrK is an acid-induced oxalate decarboxylase, *J. Bacteriol. 182*, 5271−5273.
5. Requena, L., and Bornemann, S. (1999) Barley (*Hordeum vulgare*) oxalate oxidase is a manganese-containing enzyme, *Biochem. J. 343*, 185−190.
6. Tanner, A., Bowater, L., Fairhurst, S. A., and Bornemann, S. (2001) Oxalate decarboxylase requires manganese and dioxygen for activity−overexpression and characterization of *Bacillus subtilis* YvrK and YoaN, *J. Biol. Chem. 276*, 43627−43634.
7. Woo, E. J., Dunwell, J. M., Goodenough, P. W., Marvier, A. C., and Pickersgill, R. W. (2000) Germin is a manganese containing homohexamer with oxalate oxidase and superoxide dismutase activities, *Nat. Struct. Biol. 7*, 1036−1040.
8. Anand, R., Dorrestein, P. C., Kinsland, C., Begley, T. P., and Ealick, S. E. (2002) Structure of oxalate decarboxylase from *Bacillus subtilis* at 1.75 Å resolution, *Biochemistry 41*, 7659−7669.
9. Just, V. J., Stevenson, C. E. M., Bowater, L., Tanner, A., Lawson, D. M., and Bornemann, S. (2004) A closed conformation of *Bacillus subtilis* oxalate decarboxylase OxdC provides evidence for the true identity of the active site, *J. Biol. Chem. 279*, 19867−19874.
10. Opaleye, O., Rose, R. S., Whittaker, M. M., Woo, E. J., Whittaker, J. W., and Pickersgill, R. W. (2006) Structural and spectroscopic studies shed light on the mechanism of oxalate oxidase, *J. Biol. Chem. 281*, 6428−6433.
11. Emiliani, E., and Riera, B. (1968) Enzymatic oxalate decarboxylation in *Aspergillus niger*: II. Hydrogen peroxide formation and other characteristics of the oxalate decarboxylase, *Biochim. Biophys. Acta 167*, 414−421.
12. Chang, C. H., Svedruzic, D., Ozarowski, A., Walker, L., Yeagle, G., Britt, R. D., Angerhofer, A., and Richards, N. G. J. (2004) EPR spectroscopic characterization of the manganese center and a free radical in the oxalate decarboxylase reaction−identification of a tyrosyl radical during turnover, *J. Biol. Chem. 279*, 52840−52849.

13. Begley, T. P., and Ealick, S. E. (2004) Enzymatic reactions involving novel mechanisms of carbanion stabilization, *Curr. Opin. Chem. Biol. 8*, 508−515.
14. Svedruzic, D., Jonsson, S., Toyota, C. G., Reinhardt, L. A., Ricagno, S., Linqvist, Y., and Richards, N. G. J. (2005) The enzymes of oxalate metabolism: unexpected structures and mechanisms, *Arch. Biochem. Biophys. 433*, 176−192.
15. Chang, C. H., and Richards, N. G. J. (2005) Intrinsic carbon-carbon bond reactivity at the manganese center of oxalate decarboxylase from density functional theory, *J. Chem. Theory Comput. 1*, 994−1007.
16. Borowski, T., Bassan, A., Richards, N. G. J., and Siegbahn, P. E. M. (2005) Catalytic reaction mechanism of oxalate oxidase (germin). A hybrid DFT study, *J. Chem. Theory Comput. 1*, 686−693.
17. Muthusamy, M., Burrell, M. R., Thorneley, R. N. F., and Bornemann, S. (2006) Real-time monitoring of the oxalate decarboxylase reaction and probing hydron exchange in the product, formate, using Fourier transform infrared spectroscopy, *Biochemistry 45*, 10667−10673.
18. Just, V. J., Burrell, M. R., Bowater, L., McRobbie, I., Stevenson, C. E. M., Lawson, D. M., and Bornemann, S. (2007) The identity of the active site of oxalate decarboxylase and the importance of the stability of active site lid conformations, *Biochem. J. 407*, 397−406.
19. Escutia, M. R., Bowater, L., Edwards, A., Bottrill, A. R., Burrell, M. R., Polanco, R., Vicuña, R., and Bornemann, S. (2005) Cloning and sequencing of two *Ceriporiopsis subvermispora* bicupin oxalate oxidase allelic isoforms: implications for the reaction specificity of oxalate oxidases and decarboxylases, *Appl. Environ. Microbiol. 71*, 3608−3616.
20. Svedruzic, D., Liu, Y., Reinhardt, L. A., Wroclawska, E., Cleland, W. W., and Richards, N. G. J. (2007) Investigating the roles of putative active site residues in the oxalate decarboxylase from *Bacillus subtilis*, *Arch. Biochem. Biophys. 464*, 36−47.
21. Angerhofer, A., Moomaw, E. W., Garcia-Rubio, I., Ozarowski, A., Krzystek, J., Weber, R. T., and Richards, N. G. J. (2007) Multifrequency EPR studies on the Mn(II) centers of oxalate decarboxylase, *J. Phys. Chem. B 111*, 5043−5046.
22. Reinhardt, L. A., Svedruzic, D., Chang, C. H., Cleland, W. W., and Richards, N. G. J. (2003) Heavy atom isotope effects on the reaction catalyzed by the oxalate decarboxylase from *Bacillus Subtilis*, *J. Am. Chem. Soc. 125*, 1244−1252.
23. Delieu, T., and Walker, D. A. (1972) An improved cathode for the measurement of photosynthetic oxygen evolution by isolated chloroplasts, *New Phytol. 71*, 201−225.
24. Bray, R. C., Lowe, D. J., Capeillere-Blandin, C., and Fielden, E. M. (1973) Trapping of short lived intermediates in enzymic reactions by rapid-freezing: combination of electron paramagnetic resonance with pulse radiolysis, *Biochem. Soc. Trans. 1*, 1067−1072.
25. Leslie, A. G. (2006) The integration of macromolecular diffraction data, *Acta Crystallogr., Sect. D: Biol. Crystallogr. 62*, 48−57.
26. Evans, P. (2006) Scaling and assessment of data quality, *Acta Crystallogr., Sect. D: Biol. Crystallogr. 62*, 72−82.
27. Collaborative Computational Project Number 4. (1994) The CCP4 suite: programs for protein crystallography, *Acta Crystallogr., Sect. D: Biol. Crystallogr. 50*, 760−763.
28. Murshudov, G. N., Vagin, A. A., and Dodson, E. J. (1997) Refinement of macromolecular structures by the maximum-likelihood method, *Acta Crystallogr., Sect. D: Biol. Crystallogr. 53*, 240−255.
29. Matthews, B. W. (1968) Solvent content of protein crystals, *J. Mol. Biol. 33*, 491−497.
30. Emsley, P., and Cowtan, K. (2004) Coot: model-building tools for molecular graphics, *Acta Crystallogr., Sect. D: Biol. Crystallogr. 60*, 2126−2132.
31. Read, R. J. (1986) Improved fourier coefficients for maps using phases from partial structures with errors, *Acta Crystallogr., Sect. A 42*, 140−149.
32. Brünger, A. T. (1993) Assessment of phase accuracy by cross validation - the free R-value - methods and applications, *Acta Crystallogr., Sect. D: Biol. Crystallogr. 49*, 24−36.
33. Laskowski, R. A., Macarthur, M. W., Moss, D. S., and Thornton, J. M. (1993) PROCHECK: a program to check the stereochemical quality of protein structures, *J. Appl. Crystallogr. 26*, 283−291.
34. Cruickshank, D. W. J. (1999) Remarks about protein structure precision, *Acta Crystallogr., Sect. D: Biol. Crystallogr. 55*, 583−601.
35. Armougom, F., Moretti, S., Poirot, O., Audic, S., Dumas, P., Schaeli, B., Keduas, V., and Notredame, C. (2006) Expresso: automatic incorporation of structural information in multiple sequence alignments using 3D-Coffee, *Nucleic Acids Res. 34*, W604−608.
36. Aguilar, C., Urzúa, U., Koenig, C., and Vicuña, R. (1999) Oxalate oxidase from *Ceriporiopsis subvermispora*: biochemical and cytochemical studies, *Arch. Biochem. Biophys. 366*, 275−282.
37. Whittaker, M. M., and Whittaker, J. W. (2002) Characterization of recombinant barley oxalate oxidase expressed by *Pichia pastoris*, *J. Biol. Inorg. Chem. 7*, 136−145.
38. Whittaker, M. M., Pan, H. Y., Yukl, E. T., and Whittaker, J. W. (2007) Burst kinetics and redox transformations of the active site manganese ion in oxalate oxidase: implications for the catalytic mechanism, *J. Biol. Chem. 282*, 7011−7023.
39. Antelmann, H., Towe, S., Albrecht, D., and Hecker, M. (2007) The phosphorus source phytate changes the composition of the cell wall proteome in *Bacillus subtilis*, *J. Proteome Res. 6*, 897−903.
40. Emiliani, E., and Bekes, P. (1964) Enzymatic oxalate decarboxylation in *Aspergillus niger*, *Arch. Biochem. Biophys. 105*, 488−493.
41. Schmalzlin, E., van Dongen, J. T., Klimant, I., Marmodee, B., Steup, M., Fisahn, J., Geigenberger, P., and Lohmannsroben, H. G. (2005) An optical multifrequency phase-modulation method using microbeads for measuring intracellular oxygen concentrations in plants, *Biophys. J. 89*, 1339−1345.
42. Geigenberger, P. (2003) Response of plant metabolism to too little oxygen, *Curr. Opin. Plant Biol. 6*, 247−256.
43. Makino, K., Mossoba, M. M., and Riesz, P. (1983) Chemical effects of ultrasound on aqueous solutions−formation of hydroxyl radicals and hydrogen atoms, *J. Phys. Chem. 87*, 1369−1377.
44. Park, J. S. B., Wood, P. M., Davies, M. J., Gilbert, B. C., and Whitwood, A. C. (1997) A kinetic and ESR investigation of iron-(II) oxalate oxidation by hydrogen peroxide and dioxygen as a source of hydroxyl radicals, *Free Radical Res. 27*, 447−458.
45. Forlani, F., Carpen, A., and Pagani, S. (2003) Evidence that elongation of the catalytic loop of the *Azotobacter vinelandii* rhodanese changed selectivity from sulfur- to phosphate-containing substrates, *Protein Eng. 16*, 515−519.
46. Guy, J. E., Abreu, I. A., Moche, M., Lindqvist, Y., Whittle, E., and Shanklin, J. (2006) A single mutation in the castor Δ^9-18:0-desaturase changes reaction partitioning from desaturation to oxidase chemistry, *Proc. Natl. Acad. Sci. U.S.A. 103*, 17220−17224.
47. Klinman, J. P. (2001) Life as aerobes: are there simple rules for activation of dioxygen by enzymes? *J. Biol. Inorg. Chem. 6*, 1−13.
48. Isse, A. A., Gennaro, A., and Maran, F. (1999) Mechanism of the dissociative electro-oxidation of oxalate in aprotic solvents, *Acta Chem. Scand. 53*, 1013−1022.
49. Azam, M., Kesarwani, M., Natarajan, K., and Datta, A. (2001) A secretion signal is present in the *Collybia velutipes* oxalate decarboxylase gene, *Biochem. Biophys. Res. Commun. 289*, 807−812.
50. Gucciardo, S., Wisniewski, J. P., Brewin, N. J., and Bornemann, S. (2007) A germin-like protein with superoxide dismutase activity in pea nodules with high protein sequence identity to a putative rhicadhesin receptor, *J. Exp. Bot. 58*, 1161−1171.

BI700947S